Published in final edited form as:
Dev Cell. 2011 March 15; 20(3): 376–387. doi:10.1016/j.devcel.2011.01.004.

piRNA-associated germline nuage formation and spermatogenesis require MitoPLD pro-fusogenic mitochondrial-surface lipid signaling

Huiyan Huang[1], **Qun Gao**[1], **Xiaoxue Peng**[1], **Seok-Yong Choi**[1,2], **Krishna Sarma**[1], **Hongmei Ren**[3], **Andrew J. Morris**[3], and **Michael A. Frohman**[1,*]

[1] Department of Pharmacology, Center for Developmental Genetics, Stony Brook University, Stony Brook, NY 11794–5140, USA

[2] Department of Biomedical Sciences, Chonnam National University Medical School, Hak-Dong, Gwangju, 501-746, Korea

[3] Division of Cardiovascular Medicine, The Gill Heart Institute, University of Kentucky, Lexington, Kentucky 40536-0200, USA

Summary

The mammalian Phospholipase D MitoPLD facilitates mitochondrial fusion by generating the signaling lipid phosphatidic acid (PA). The *Drosophila* MitoPLD homolog Zucchini (Zuc), a proposed cytoplasmic nuclease, is required for piRNA generation, a critical event in germline development. We show that Zuc localizes to mitochondria and has MitoPLD-like activity. Conversely, MitoPLD$^{-/-}$ mice exhibit the meiotic arrest, DNA damage, and male sterility characteristic of mice lacking piRNAs. The primary function of MitoPLD appears to be the generation of mitochondrial-surface PA. This PA in turn recruits the phosphatase Lipin 1, which converts PA to diacylglycerol and promotes mitochondrial fission, suggesting a mechanism for mitochondrial morphology homeostasis. MitoPLD and Lipin 1 have opposing effects on mitochondria length and on intermitochondrial cement (nuage), a structure found between aggregated mitochondria that is implicated in piRNA generation. We propose that mitochondrial-surface PA generated by MitoPLD / Zuc recruits or activates nuage components critical for piRNA production.

Introduction

Mitochondria, in addition to their long-recognized role in energy production, are now appreciated to regulate numerous cell biological pathways including apoptosis and intracellular calcium homeostasis (Lebiedzinska et al., 2009). These regulatory processes involve communication between the mitochondria and the rest of the cell via signaling pathways on the mitochondrial surface that mediate interactions with cytoplasmic proteins. Some of these pathways involve lipids (Huang and Frohman, 2009), such as cardiolipin, which serves to recruit tBid during apoptosis (Schug and Gottlieb, 2009). We previously reported that human MitoPLD, a member of the Phospholipase D (PLD) superfamily,

*Corresponding author: michael@pharm.stonybrook.edu, phone: 631-632-1476; fax: -1692.

initiates a novel lipid signaling pathway that facilitates mitochondrial fusion (Choi et al., 2006). Mitochondrial fusion and fission are important for many aspects of normal cellular homeostasis, enabling mitochondria to alter their morphology to increase the efficiency of energy production, to mark unhealthy mitochondria for autophagy, and to translocate to subcellular locations at which ATP generation or calcium uptake are most needed (Chen and Chan, 2009). The rates of fusion and fission are regulated by varied types of signaling events.

MitoPLD is a highly divergent PLD superfamily member most closely related to a subfamily of prokaryotic PLDs collectively called Nuc, which function as endonucleases (Choi et al., 2006). However, unlike Nuc, MitoPLD was unexpectedly found, using biochemical approaches, to cleave the mitochondrial-specific lipid cardiolipin to generate the canonical PLD superfamily product Phosphatidic Acid (PA). PA, a pleiotropic and rapidly metabolized signaling lipid, has been shown to function as a membrane anchor for recruitment of SNARE complex proteins, small G-protein exchange factors and kinases, to activate lipid kinase enzymes and vesicle trafficking machinery, and to serve as substrate for production of the signaling lipids diacylglycerol (DAG) and lysoPA (Cazzolli et al., 2006; Jenkins and Frohman, 2005). Overexpression of wild-type MitoPLD causes mitochondria to aggregate, whereas a catalytically-inactive allele or RNAi knockdown decreases fusion resulting in mitochondrial fragmentation. This indicates that it is the production of PA that regulates mitochondrial morphology, rather than protein:protein interactions or other potential roles for MitoPLD (Choi et al., 2006). Nonetheless, the mechanism through which MitoPLD-generated PA alters mitochondrial morphology remains unknown.

The *Drosophila* homolog of MitoPLD, denoted Zucchini (Zuc), has been reported to be a cytoplasmic presumptive nuclease with a critical role in piRNA generation during gametogenesis (Pane et al., 2007). piRNA, a germline-specific defense mechanism against transposon mobilization, is generated via a pair of multi-protein complexes with distinct subcellular localization (Aravin et al., 2009). One complex, termed the pi-body, localizes to one type of an electron-dense structure known as nuage (Russell and Frank, 1978). This type of nuage is transiently associated with aggregated mitochondria in gametogenesis shortly before and during meiosis. The other complex, the piP-body, is physically distinct but in nearby germinal cytoplasmic granules. piRNAs are thought to be generated initially by the pi-body (primary piRNAs), following which the piP-body amplifies and expands the piRNA population generated (Brennecke et al., 2007). Zuc is involved in the production of the primary piRNAs characteristic of the pi-body, although whether it is required (Saito et al., 2009) or has a more modest role (Malone et al., 2009) in primary piRNA generation remains unsettled. Loss of Zuc, or most any other of the identified piRNA pathway components in either complex, results in a failure to suppress transposon mobilization, ensuing DNA damage, and check point-induced meiotic arrest, leading to apoptosis and sterility (Thomson and Lin, 2009), although Zuc may undertake other roles as well (Pane et al., 2007). A number of piRNA pathway components, when ablated in mice, create similar phenotypes, leading to meiotic arrest during spermatogenesis (He et al., 2009).

Taken together, these reports raised questions regarding whether the mammalian and *Drosophila* MitoPLD/Zuc homologs have evolved to undertake different enzymatic functions at different subcellular locations, or whether MitoPLD/Zuc might encode multiple types of activities and functions. We present findings in this report that largely resolve the species differences, indicating conserved roles in mitochondrial lipid signaling, fusion/fission homeostasis, and meiotic progression. Moreover, we extend this lipid signaling pathway to encompass diacylglycerol (DAG), which appears to play an opposing role in both mitochondrial morphology and nuage formation. Our results suggest a link between mitochondrial dynamics and the germline ultrastructure necessary for piRNA production.

Results

Both human and *Drosophila* MitoPLD/Zuc alter mitochondrial morphology in an activity-dependent manner and localize to mitochondria

As previously reported, the mechanism via which MitoPLD becomes localized to mitochondria involves a 39-amino acid N-terminal domain that functions as a trans-membrane tail to anchor MitoPLD into the outer mitochondrial membrane (Choi et al., 2006). *Drosophila* Zuc also encodes a predicted N-terminal trans-membrane mitochondrial localization sequence (Choi et al., 2006), but was reported to localize to cytoplasmic granules and to peri-nuclear cytoplasm including the nuage (Pane et al., 2007; Saito et al., 2009), potentially through complex formation with the nuage-localized piRNA-binding protein Aubergine (Pane et al., 2007). However, these studies employed Zuc alleles N-terminally tagged with EGFP or HA. We thus examined the possibility that the Zuc mitochondrial localization sequence had been inactivated in the N-terminal fusion protein.

Mitochondria in HeLa cells characteristically appear as an elongated and branched tubular network (Fig. 1A, arrow). Overexpressed Wild-Type (WT) human MitoPLD tagged C-terminally with EGFP localizes to the mitochondria and causes them to accumulate peri-nuclearly as an aggregate (Fig. 1A, *; region denoted by diamond shown magnified in inset). In contrast, catalytically-inactive MitoPLD (H156N) triggers mitochondrial fragmentation (Fig. 1B, arrowhead, inset), which also frequently results in peri-nuclear accumulation. Deleting the N-terminal domain (Fig. S1) or placing EGFP at the N-terminus (Fig. 1C) causes MitoPLD to localize to the cytoplasm and prevents changes to mitochondrial morphology. Finally, in contrast to the published reports (Pane et al., 2007;Saito et al., 2009), *Drosophila* Zuc tagged C-terminally with EGFP localizes to mitochondria (Fig. 1D, arrow), and like WT-MitoPLD, triggers perinuclear aggregation when overexpressed sufficiently (*). Conversely, an inactive allele of Zuc, H169N, causes fragmentation (Fig. 1E, arrowhead).

Taken together, these findings indicate that, like human MitoPLD, Zuc localizes to mitochondria. Moreover, it stimulates mitochondrial aggregation in an activity-dependent manner.

MitoPLD produces PA on the mitochondrial surface

We previously reported, using biochemical approaches, that MitoPLD hydrolyzes cardiolipin to generate PA (Choi et al., 2006), raising the question of where on the mitochondria the PA is generated and accumulates. A fluorescent sensor for PA (Raf1-PA Binding Domain (PABD)-EGFP, Rizzo et al., 2000) was employed to visualize changes in detectable PA as a consequence of manipulating the MitoPLD expression level. In control NIH3T3 cells, the sensor distributes throughout the cell (Fig. 2A). However, increasing MitoPLD expression to cause PA production induced sensor translocation to the aggregated mitochondria (Fig. 2B, arrow). The recruitment was specific for PA, since increasing MitoPLD expression did not elicit translocation of a mutant form of the PA sensor that lacks the ability to bind PA (Fig. S2A,B), nor did the wild-type sensor translocate in response to expression of the catalytically-inactive MitoPLD allele H156N (not shown). Finally, the PA sensor did not translocate to the mitochondrial surface when the N-terminally-truncated, cytosolic wild-type allele (Δ39-MitoPLD) was expressed, indicating a requirement for MitoPLD to be localized to the mitochondrial surface for PA to be generated there (not shown). Detection of PA on the exofacial mitochondrial surface supports our prior model that MitoPLD is an outer membrane protein with a cytoplasmically-oriented catalytic domain that hydrolyzes CL on the mitochondrial surface (Choi et al., 2006).

MitoPLD production of PA recruits Lipin 1b which converts the PA into DAG

In many signaling events, the PA produced by PLD is rapidly converted to DAG. This process either serves to terminate the signaling events promoted by PA, or DAG itself is the bioactive signaling lipid in the cell biological process (Brindley et al., 2009). We thus sought to determine if MitoPLD-generated PA is converted to DAG, the enzyme involved if so, and whether accelerating the conversion of PA to DAG promoted or opposed the pro-fusion effects of PA, since DAG has been linked both to membrane organelle fusion and fission events in different settings (Riebeling et al., 2009). PA dephosphorylation to generate DAG is mediated by the Type 1 and 2 families of phosphatidate phosphatases (PAPs). PAP2s are well established as multipass transmembrane proteins with active sites on the extracellular surface or lumen of organelles, making them unlikely candidates to mediate cytosolic conversion of PA to DAG. PAP1, on the other hand, was recently identified as the Lipin family of cytosolic proteins. Lipin 1 (of three isoforms) is the best studied family member (Brindley et al., 2009). Mutations in Lipin 1 cause a Type-II diabetes-like syndrome in mice called fatty liver dystrophy (fld) that involves lipid storage dysregulation and poorly understood abnormal mitochondrial function. The localization of Lipin 1 is complex, including to the cytoplasm, endoplasmic reticulum, nuclear envelope, and nucleus in different cell types and settings. The two alternately spliced isoforms Lipin 1a and 1b (see Fig. 3) may have differences in their localization patterns.

Transfection of Lipin 1b into NIH3T3 cells revealed a punctate cytoplasmic localization (Fig. 2C). Surprisingly, increased expression of MitoPLD resulted in translocation of virtually all of the Lipin 1b to the aggregated mitochondria (Fig. 2D, arrow). The translocation was not due to physical interaction between MitoPLD and Lipin 1b, since increased expression of catalytically-inactive MitoPLD did not recruit Lipin 1b to the mitochondrial surface (Fig. 2E). The translocation was also not caused by mitochondrial aggregation *per se*, since forcing aggregation through overexpression of the fusion protein Mitofusin 1 (Chen et al., 2003), which does not substantially elevate mitochondrial PA levels (Choi et al., 2006), did not elicit Lipin 1b movement (Fig. 2F). Finally, underscoring the direct role of PA in the recruitment, Lipin 1b could alternately be recruited to the plasma membrane by overexpression of Phospholipase D2 (Fig. S2C, D), a mammalian PLD that generates PA on the plasma membrane via hydrolysis of phosphatidylcholine (Colley et al., 1997).

We next employed a fluorescent sensor for DAG (C1bδ-YFP, Giorgione et al., 2006) to determine whether Lipin 1b, once brought to the mitochondrial surface, would generate DAG from the PA available there. When expressed in NIH3T3 cells, which express relatively low levels of Lipin 1b, the sensor localizes in part to the Golgi apparatus (Fig. 2G), a site at which DAG is abundant. Increased expression of MitoPLD alone did not cause substantial translocation of the sensor to mitochondria (Fig. 2H). However, increased expression of both MitoPLD and Lipin 1b led to robust translocation of the DAG sensor to the aggregated mitochondria (Fig. 2I). Biochemical analysis revealed a 75% increase in DAG in mitochondria prepared from Hela cells overexpressing MitoPLD and Lipin 1b compared to control Hela mitochondria (from 9.6×10^6 to 16.8×10^6 pmol DG / phosphate), although this approach does not reveal the specific increase on the mitochondrial surface. The increase in mitochondrial surface DAG was dependent on the catalytic activity of Lipin 1b, since the catalytically-inactive allele D712A (Brindley et al., 2009) efficiently translocated to mitochondria overexpressing MitoPLD but did not trigger recruitment of the DAG sensor (Fig. S2E,F). Taken together, these results demonstrate that in a setting of exaggerated expression, Lipin 1b moves to the mitochondrial surface in response to MitoPLD-generated PA and converts it into DAG (Fig. 2J).

Lipin 1b is recruited to mitochondria via a PA-responsive central domain and decreases mitochondrial length

Transient expression of Lipin 1b in HeLa cells transformed the characteristic long mitochondrial tubules (Fig. 3A, arrow) into moderately-sized fragments (Fig. 3A, asterisk). Quantitation of the shift revealed a statistically significant shift towards fragmentation, but only for the wild-type Lipin 1b allele, not for the catalytically-inactive one (Fig. 3B). Conversely, Lipin 1 knock-down lengthened mitochondrial tubules (Fig. 3C). Mitochondria in control NIH3T3 cells infected with adenoviral-delivered LacZ shRNA were intermediate (63±14%; arrowheads) or tubular (36±13%) in appearance, with only 1% exhibiting an elongated, super-tubulated morphology. In contrast, 35%±7% of the mitochondria in cells infected with Lipin shRNA (Finck et al., 2006) were unusually elongated (arrows), and many fewer cells were intermediate in morphology (23±7%). These findings suggest that PA is the pro-fusogenic lipid signal, and Lipin 1b conversion of PA to DAG serves to terminate the pathway(s) activated by PA. The results also indicate that Lipin 1b affects mitochondrial morphology at physiological levels of PA, although the fraction of Lipin 1b stably recruited to the mitochondria in this setting is below the limit of visible detection using this microscopic approach.

These findings raised the issue of the PA-directed recruitment mechanism. Lipin 1b encodes a C-terminal catalytic domain, a conserved N-terminal LIP domain of unknown function, and three basic amino acid-rich regions characteristic of the types of unstructured, positively-charged regions that mediate binding of a number of signaling proteins to PA (Fig. 3D). Deletion analysis revealed that none of these domains and regions mediated the recruitment, but rather, the translocation was regulated by a central domain, amino acids 430–570 (Fig. 3D, E and data not shown). As before, neither catalytically-inactive MitoPLD nor Mitofusin 1 triggered mitochondrial translocation (Fig. S3A, B), and the Lipin 1b PA-responsive central domain could be recruited to the plasma membrane by increased expression of PLD2 (Fig. S3C, D). Although there is no obvious cluster of basic amino acids in this central region, there are dispersed basic amino acids that may mediate interaction with PA. Alternately, it is possible that this region may interact with another protein that binds PA directly. However, since the region also translocates to the plasma membrane upon PLD2 expression, such a hypothetical protein partner could not be mitochondrial-specific.

The Lipin 1 catalytic domain localizes to sites of mitochondrial fission and promotes fission in a PA-independent manner

Unexpectedly, even though elevated levels of PA on the mitochondrial surface are required to recruit a visibly detectable quantity of full-length Lipin 1b, the isolated Lipin 1 catalytic domain (amino acids 705–924) localized to mitochondria in cells with physiological levels of PA (Fig. 4A, arrow) and caused production of DAG (Fig. S4A). In fact, the Lipin 1 catalytic domain localized to mitochondria even in cells expressing catalytically-inactive MitoPLD, which should lack or have markedly decreased PA on the mitochondrial surface (Fig. S4B). Moreover, the normally elongated mitochondrial tubules characteristic of HeLa cells (Fig. 4A, asterisk) exhibited almost complete fragmentation (Fig. 4A, arrow), and the Lipin 1 catalytic domain localized to the tips of the small mitochondria (Fig. 4B). In rare cells in which the fragmentation was incomplete, the Lipin 1 catalytic domain was observed to localize in a punctate manner on the tubules (Fig. 4C, D), which was reminiscent of the localization pattern for Drp1, a protein that drives mitochondrial fission (Frank et al., 2001). Localization of Drp1 and the Lipin 1 catalytic domain on the incompletely fragmented tubules (Fig. 4E, Fig. S4C) revealed that the Lipin 1 catalytic domain (Fig. 4I) co-localized with Drp1 (Fig. 4J) at constricted regions of the tubules (Fig. 4F-H, arrowheads), suggesting its participation in the fission process. However, there were also numerous sites of tubular constriction at which Drp1 alone was found (arrows).

These findings suggest a model in which fusion events involving MitoPLD lead to PA production on the mitochondrial surface (Fig. 4L), which recruits Lipin 1b. We propose that the recruitment process induces a conformational change in Lipin 1b that exposes the cryptic, fission site-localizing domain, leading to focusing of Lipin 1b at future sites of fission through interaction with an unknown protein partner, and promotion of fission through production of DAG. This hypothetical model is attractive for several reasons, including that PA has been shown in biochemical assays to dramatically stimulate Lipin 1 catalytic activity through an unknown mechanism (Han and Carman, 2010). Moreover, mitochondrial fusion events have been linked temporally and spatially to future fission events, although the underlying mechanism is unknown (Liu et al., 2009;Twig et al., 2008). The model proposed here provides one such potential mechanism via a process that would promote homeostasis, i.e., mitochondria undergoing fusion would stimulate their own future fission, helping to maintain mitochondria within a relatively restricted range of sizes.

Mouse embryo fibroblasts lacking MitoPLD exhibit shortened mitochondrial tubules and fragments and are resistant to the effects of Lipin 1b but not the Lipin 1 catalytic domain

We targeted the MitoPLD gene in embryonic stem cells to generate an allele in which the second exon, which encodes the key HKD catalytic motif, was flanked with loxP sites (Fig. S5). Mice harboring the targeted allele were crossed to mice expressing Cre recombinase in oocytes, and off-spring with Cre-deleted alleles identified. Mice heterozygous for the Cre-deleted allele were mated to generate homozygous mice that express only the first exon (MitoPLD$^{-/-}$), which should constitute a complete loss of gene function, since the HKD motif is critical for enzymatic activity for all members of the PLD superfamily (Jenkins and Frohman, 2005).

Mouse embryo fibroblasts (MEFs) were isolated from MitoPLD$^{-/-}$ and control WT E13.5 embryos. Control MEFs almost uniformly exhibited long, tubular mitochondria (Fig. 5A, quantitation in 5C), whereas MitoPLD$^{-/-}$ MEFs exhibited shortened mitochondria (Fig. 5B, square inset), and in almost half of the cells, mitochondrial fragments (arrow) were particularly prominent in the cellular periphery (Fig. 5B, enhanced in round inset). This finding confirms a role for MitoPLD in regulation of mitochondrial morphology, although the phenotype is less profound than that observed for loss of proteins that physically mediate the fusion event such as Mitofusin 1 (Chen et al., 2003).

Similar to the results shown in Fig. 3A and B for HeLa cells, expression of Lipin 1b in WT MEFs led to mitochondrial shortening and fragmentation (74.6% reduction in tubulation, 238% increase in fragmentation, n=336 total cells counted, $p<0.001$). However, Lipin 1b expression did not result in further shortening or fragmentation of MitoPLD$^{-/-}$ MEFs (n=346, $p>0.15$). In contrast, the Lipin 1 catalytic domain efficiently triggered fragmentation for both WT and MitoPLD$^{-/-}$ MEFs (Fig. 5D, E). Taken together, these results confirm that the ability of full-length Lipin 1b to promote mitochondrial fission is dependent on PA production by MitoPLD, but the isolated catalytic domain functions independently of PA production.

MitoPLD$^{-/-}$ mice exhibit meiotic arrest during spermatogenesis, loss of nuage and TDRD1, and genomic damage

MitoPLD$^{-/-}$ offspring generated by crossing MitoPLD$^{+/-}$ mice were born in the normal Mendelian ratio and appeared grossly normal. Mating of the MitoPLD$^{-/-}$ male and female mice revealed normal fertility for females, but 100% penetrant infertility for male mice (> 7 males continuously mating for 6 months). We previously reported that MitoPLD is expressed widely at low levels (Choi et al., 2006), and many ESTs in the NCBI database have been isolated from brain and lung. An anti-MitoPLD antiserum demonstrated

expression of MitoPLD in the adult testes (Fig. 6A). Data available from microarray studies revealed that MitoPLD is expressed at low levels in type A and B spermatogonia, increases 5-fold in spermatocytes undergoing meiosis (pachytene spermatocytes), and then decreases again in round spermatids, and that it is expressed at low levels in testes in young mice, and then increases 7-fold from day 14 to day 29 with the onset of puberty (Fig. S6).

Gross histological examination demonstrated a substantial reduction in size for MitoPLD$^{-/-}$ testes obtained from 3-month old mice (Fig. 6B, C). Hematoxylin and eosin staining of fixed sections revealed a dramatic difference in morphology. Seminiferous tubules in WT testes exhibited normal architecture with an external layer of spermatogonia (Fig. 6D) and progressively more differentiated spermatocytes (Fig. 6E, a,b) and finally spermatids (Fig. 6E, c) towards the lumen of the tubule. In contrast, MitoPLD$^{-/-}$ tubules were reduced in size with only a thin layer of cells around the periphery (Fig. 6D, E). Spermatogonia and Sertoli cells appeared normal (Fig. 6E, d), and spermatocytes early in meiosis (prophase) at the leptotene / zygotene / early pachytene stages were observed (Fig. 6E, e), but not late or post-meiotic spermatocytes nor spermatids. Instead, the tubules contained many cells with condensed, heavily staining nuclei typical of cells undergoing apoptosis (Fig. 6E, f, lower cell), cells with disorganized chromosomal material (Fig. 6D, arrowhead, inset; 6E, f, upper cell), vacuoles suggestive of cell drop-outs (Fig. 6D, asterisks), and cell debris sloughed into the lumen of the tubules (Fig. 6D, upper left). These findings indicate that spermatocytes in MitoPLD$^{-/-}$ mice exhibit meiotic arrest, consistent with the phenotypes for *zuc*$^{-/-}$ *Drosophila* and for a number of genes involved in piRNA production that have been shown to be required for mammalian spermatogenesis.

Electron microscopy examination of spermatocytes from wild-type mice at the prophase stage revealed numerous cells in which the mitochondria were aggregated peri-nuclearly (Fig. 6F, arrowheads; Fig. S6B), separated by electron-dense nuage, also known as intermitochondrial cement (Fig. 6G, arrow; higher magnification in H). Nuage and aggregated mitochondria were observed in all wild-type samples examined. In contrast, neither aggregated mitochondria nor associated nuage were observed in any sample of multiple MitoPLD$^{-/-}$ testes examined (Fig. 6I). Mitochondria could be found on occasion in close approximation (Fig. 6J), but they were not separated by interposed nuage (Fig. 6K). Loss of nuage is characteristic of some, but not all, of the previously reported knockout phenotypes for piRNA components that cause meiotic arrest (He et al., 2009).

piRNA components are known to form large multi-protein complexes, which has led to the hypothesis that loss of critical proteins physically destabilizes the entire complex (Ma et al., 2009). MitoPLD could be proposed to undertake a similar function. However, this appears unlikely, since one of the fully penetrant alleles of *Drosophila zuc* is a mutation of the key histidine in the HKD enzymatic motif (Pane et al., 2007), which should only eliminate enzymatic activity. We have shown that mutation of this residue results in a mutant protein (for both *Drosophila* Zuc and human MitoPLD) that is expressed at wild-type levels, localizes normally to the mitochondria, and folds sufficiently well to heterodimerize with wild-type protein and function as a dominant negative (Fig. 1, and Choi et al., 2006). Thus, a critical protein:protein interaction does not seem likely to underlie the requirement for MitoPLD in formation of nuage-associated mitochondria. In fact, overexpression of enzymatically-active MitoPLD in cultured cell lines aggregates mitochondria with a thin intervening layer of electron dense material (Fig. 6L,M, and Choi et al., 2006), suggesting that the formation of nuage-associated mitochondria might be driven solely by raising levels of PA sufficiently high enough on the surface of the mitochondria, since almost all of the other piRNA-associated components are expressed only in germ cells and hence would not be present in the cultured cells.

Loss of nuage should result in mislocalization or loss of critical pi-body components of the piRNA pathway. To examine this, immunofluorescent staining for TDRD1, one such component, was performed. TDRD1 expression initiates in the meiotic prophase as spermatogonia differentiate into spermatocytes, and then decreases with formation of spermatids (Hosokawa et al., 2007). TDRD1 localized to the nuage, which appeared as a collection of largely peri-nuclear punctate foci in spermatocytes in WT tubules prepared from adult male mice (Fig. 7A). In contrast, TDRD1 was not detected in MitoPLD$^{-/-}$ tubules (Fig. 7B).

Loss of critical components of the piRNA-generating pathway, such as TDRD1, leads to transposon mobilization and ensuing DNA damage, as can be visualized by imaging γH2X which localizes to double-strand DNA breaks (Soper et al., 2008). A low level of γH2X expression is observed in WT tubules as a consequence of the meiotic process and a low level transposon expression (Fig. 7C and Soper et al., 2008). Markedly increased levels of γH2X were observed in MitoPLD$^{-/-}$ spermatocytes (Fig. 7D), indicative of substantial genomic damage. Taken together, the loss of nuage and TDRD1, increased genomic damage, meiotic arrest, and cell death provides compelling evidence that the role of MitoPLD in mice is similar to the role of Zuc in *Drosophila* in the piRNA generation pathway that confers defense against transposon mobilization during gametogenesis.

Ablation of the PA-metabolizing enzyme Lipin 1 increases nuage and alters the localization pattern of TDRD1

Male mice lacking Lipin 1 (*fld*, fatty liver dystrophy) are infertile, which has been proposed to ensue from their spastic neurological phenotype (Langner et al., 1991). Examination of adult *fld/fld* testes indicated that they are normal sized, appear normal histologically, and produce motile sperm (not shown). However, electron microscopy examination revealed a difference in the appearance of nuage (Fig. 7E, arrowheads). In contrast to the nuage observed in WT mice (Fig. 6F-H), which exhibited approximately the same density as the adjacent mitochondrial matrix (Figs. 6F, 7H), the nuage in *fld/fld* spermatocytes was substantially increased in density (Fig. 7E–H). In addition, the nuage between mitochondria in WT mice typically was short in length (17.6% ± 2.9% of the circumference of the mitochondria, n=11), but was 2-fold longer for *fld/fld* spermatocytes (34.3% +2.7%, n=18, $p<0.01$). Consistent with the alteration in nuage appearance, the localization of TDRD1 was also altered, in that the pattern of many small foci shifted to a less uniform collection dominated by larger foci (Fig. 7I, J). Taken together, these findings suggest that loss of the PA-metabolizing enzyme Lipin 1 results in elevated levels of PA on the mitochondrial surface, leading to increased nuage formation and further supporting the role of PA in mitochondria - nuage association.

Discussion

The piRNA generation pathway is complex, involving enzymes that methylate the RNA-cleaving enzymes and piRNAs themselves, mRNAs that both serve as substrate to generate piRNAs and encode proteins that transport the piRNAs to the nucleus, and proteins of unknown function that may serve as scaffolds or recruit small G-proteins to the active complex. piRNA primary processing takes place on pi-bodies, which co-localize with intermitochondrial cement / nuage (Russell and Frank, 1978). A current question concerns the relationship of the primary processing in pi-bodies to the association of nuage with mitochondria. We show here that a mitochondrial regulator of fusion/fission homeostasis is also required for nuage formation and meiotic progression. In the accompanying report by Watanabe et al., a meotic spermatogenic block and a requirement for MitoPLD in nuage formation is similarly shown, accompanied by loss of the majority of primary piRNA biogenesis and derepression of LINE1 retrotransposons in the mutant testis. Zucchini, the

Drosophila homolog of MitoPLD, was reported as a cytoplasmic or nuage-localizing presumptive nuclease (Pane et al., 2007). As previously reported, we were unable to demonstrate nuclease activities for MitoPLD (Choi et al., 2006). Instead, we found that it generated a lipid signal using the mitochondrial lipid cardiolipin as substrate to generate PA, although we can not formally rule out the possibility that MitoPLD might additionally display piRNA-generating nuclease activities in the presence of the proteins and environment found in spermatocytes. Nonetheless, we show here that Zuc, when not N-terminally tagged, localizes to mitochondria and alters mitochondrial morphology, including causing mitochondrial aggregation, prompting the need for new hypotheses concerning how it regulates piRNA generation in *Drosophila*.

We showed previously that MitoPLD generates PA in the context of fusion events (Choi et al., 2006). We show here the PA is generated on the mitochondrial surface, and that the PA recruits a second lipid-modifying enzyme, Lipin 1, to convert the PA into DAG, which then promotes fission. DAG has been shown to regulate fission of membrane vesicles at the Golgi via recruitment of Protein kinase D or through effecting changes in membrane curvature {Bossard, 2007 #301; Fernandez-Ulibarri, 2007 #302; Shemesh, 2003 #303}, but has not previously been linked to mitochondrial fission. The spatiotemporal linkage of fusion and fission we propose is intriguing in light of two prior reports. Twig *et al*. (Twig et al., 2008) have described a temporal correlation between fusion and fission: mitochondria fuse at random points on average every 10 minutes, but many fusion events are followed rapidly (average, 70 seconds) by a fission event. This “kiss and run” type of (partial) fusion event can be discriminated from full fusion events by rapid assembly of Drp1 at the fusion site, followed by fission (Liu et al., 2009). The lipid signaling pathway we describe here suggests potential mechanisms through which such temporal-spatial targeting of fission could be achieved. Conversely, sites at which only Drp1 assembly is observed (Fig. 4) may represent fission events spatially and temporally unconnected to fusion events. The effects of MitoPLD and Lipin on mitochondrial morphology are likely to have consequences for tissues in which regulated fusion and fission are important, including in peripheral tissues such as fat and muscle. Alterations in mitochondrial fusion and fission could lead to changes in numbers of mitochondria and potentially the capacity for fatty acid oxidation. However, the effects do not trigger lethality. This is frequently the case for lipid signaling genes for which compensatory mechanisms can moderate the loss of a single synthetic or degradative pathway. Two other Lipin genes and another MitoPLD-related gene are present in the mammalian genome and may provide some redundancy or compensation in the long-term knockout setting.

However, the dramatic effect of loss of MitoPLD / Zuc on nuage association with mitochondria and piRNA-generation raises the question of the enzymatic role played by these enzymes, presumably though generating the lipid signal PA. Examination of mice lacking Lipin 1 revealed more, not less nuage, and mature sperm were produced, suggesting that PA is the bioactive lipid in this process rather than DAG, which is the key signaling lipid in other well-defined signaling pathways (Mor et al., 2007). PA is well established as a lipid anchor that recruits a variety of types of proteins with PA-binding domains and/or activates enzymes such as kinases (Jenkins and Frohman, 2005). The apparent requirement for PA in this setting is reminiscent of the role of yeast PLD (Spo14) during meiosis, where it localizes to an electron-dense amorphous structure on the outer surface of spindle pole bodies, and, through generating PA there, recruits a PA-binding protein that is key for the subsequent developmental step (Nakanishi et al., 2006). Could MitoPLD / Zuc -generated PA play an analogous role? One possibility is that the PA might recruit a key protein required for piRNA production to the nuage. We have examined whether proteins known to be critical in the pathway, Miwi, Mili, MVH, Tdrd1, Tdrd6, Tdrkh (Tdrd2), Gasz, and RanBP9, are recruited to the mitochondria in HeLa cells overexpressing MitoPLD, but did

not observe PA-induced translocation (not shown). It is possible that formation of the proteins into a complex is required to expose a PA-binding domain, or that there is a PA-responsive critical protein in the pathway that we have not yet examined. Alternately, nuage has long been known to be strongly positively charged (Paniagua et al., 1985), due presumably to the high content of ribonucleoproteins. Since PA is a strongly negatively charged lipid, mitochondria with exofacial PA might simply be able to associate with and sandwich nuage via electrostatic interactions. A regulatory function for PA would still be required, but could involve conformational change or activation of some component of the piRNA-generating process through proximity with PA, rather than robust recruitment.

Finally, we report two functional roles for MitoPLD, one involving relatively low level expression that has effects on mitochondrial morphology in non-germ cells, and another involving high level expression that leads to mitochondrial aggregation. The mechanism underlying MitoPLD effects on mitochondrial morphology and fusion are unknown but may involve promoting transient outer leaflet trans-affinity to facilitate fusion and thus represent a weaker version of the role undertaken by MitoPLD during spermatogenesis.

Experimental Procedures

Plasmid construction

Truncation mutants of HA-tagged mouse Lipin 1b were generated by amplifying the specified region using PCR and ligating the restriction enzyme-digested PCR products into an expression vector containing a 3xHA tag. Site-directed mutagenesis was performed using the Quik-Change kit (Invitrogen). Successful mutagenesis and integrity of the remainder of the coding region was confirmed by sequencing. Details of construction of plasmids described in this study will be provided upon request.

Cell culture and transfection

MEF, HeLa and NIH3T3 cells were maintained in DMEM (Invitrogen, Carlsbad, CA) supplemented with 10% calf serum (Hyclone, Logan, UT). NIH3T3 cells stably transfected with mifepristone-inducible WT and H156N MitoPLD and Mitofusin1 were generated previously (Choi et al., 2006). CHO cells stably transfected with tetracycline-inducible PLD2 were generated previously (Du et al., 2004). NIH3T3, MEF and CHO cells were transfected with Lipofectamine LTX (Invitrogen, Carlsbad, CA) according to the manufacturer's instructions. HeLa cells were transfected using FuGene HD (Roche) transfection reagent.

Immunofluorescence microscopy

24 hours after transfection, cells were fixed with 4% paraformaldehyde for 15 min, permeabilized with 0.1% Triton X-100 for 10 min, and blocked with 5% normal goat serum for 1 hour. The cells were then immunostained using primary antibodies against cytochrome c (1:200, Pharmingen, San Diego, CA), HA epitope (1:500, Rockland Immunochemicals, Gilbertsville, PA), calreticulin (1:500, Stressgen Biotechnologies, San Diego, CA), GM130 (1:500, BD Transduction Laboratory), FLAG epitope(1:500, M2; Sigma, St Louis MO), and Drp1 (1:200, BD Transduction Laboratory) followed by fluorescent dye-conjugated secondary antibodies (1:500). Stained cells were visualized using a Leica TCS2 or Zeiss 510 confocal microscope. Images were processed using Adobe Photoshop.

Western Blotting

Freshly isolated adult mice testes were snap-frozen in liquid nitrogen, pulverized in dry ice using a precooled motor, and lysed in 8M urea lysis buffer. Samples were centrifuged and the supernatant used for both Western-blot analysis (40 μg of protein) on 10% SDS-PAGE,

and measurement of protein concentration. After transfer to nitrocellulose membrane, blots were probed with primary antibody, followed by secondary antibodies conjugated with IRDye 800 (Rockland Immunochemicals, Gilbertsville, PA). Fluorescent signals were detected with an Odyssey infrared imaging system (LICOR Biosciences, Lincoln, NB).

Polyclonal anti-MitoPLD antibody was custom made by Covance (PA, U.S.A) using the synthetic peptide CIGLLRKAGIQVRHDQD as antigen. The resulting antiserum was affinity-purified using a peptide-bead coupled column. The antiserum only weakly recognizes native MitoPLD when overexpressed in cell lines, contains cross-reacting antibodies that stain the Golgi and nucleoli, and does not exhibit sufficient signal:noise sensitivity to image endogenous MitoPLD in spermatocytes.

Mitochondrial morphology quantification

Mitochondrial morphology was visualized by staining with anti-cytochrome c antibody and imaging using confocal microscopy. Morphology of mitochondria for each cell was then categorized by a blinded investigator into tubular (more than 75% of mitochondria with long tubules), intermediate (25–75% mitochondria with long tubules) and fragmented (only 25% or less mitochondria with long tubules). Long tubules were defined as > 5 μm in length.

Generation of MitoPLD$^{-/-}$ mice

MitoPLD gene-targeted mice were generated using homologous recombination of C57/Bl6 stem cells as described in Fig. S5, by Ozgene (Australia). C57/Bl6 blastocyst embryos were used for generation of germline transmitted heterozygous mice, and Cre-recombinase was introduced using an egg-driven Cre gene in a C57/Bl6 background. The resulting offspring were genotyped to discard the Cre gene and maintained as heterozygotes. Genotyping was performed using PCR primers P1, 2, and 3 as shown in Fig. S5. P1: gttagccagccaaagccagtgtg; P2: atggcctgtgtggtccagttgag; P3: tgatacaagaggggtggatgtccac. Animal procedures were approved by the SBU Institutional Animal Care and Use Committee (IACUC).

Generation of primary and immortalized MEFs

MEFs were prepared from embryos derived from intercrossing MitoPLD$^{+/-}$ heterozygotes at embryonic day 13.5 after fertilization. Primary WT or knockout MEFs were immortalized by transfecting cells with an SV40 large T antigen expressing construct. Genotyping was done by PCR using the primers P1–3 described above.

Histology

Freshly dissected testes were fixed in 4% paraformaldehyde overnight at 4°C, processed for paraffin embedding, sectioned at a thickness of 5μm, and stained with hematoxylin and eosin.

Immunofluorescence on sections

10μm cryosections of testes were fixed in 4% paraformaldehyde and immunostained with anti-TDRD1 (Abnova) or anti-phospho-histone-H2A.X (Ser 139) (Millipore) antibody, followed by secondary antibody Alexa Fluor 568 anti-mouse IgG. Nuclei were stained with DAPI.

Electron Microscopy

Samples used for transmission electron microscopy were processed using standard techniques. Briefly, 2–5 month old mice were perfused with 4% paraformaldehyde and 2.5% EM grade glutaraldehyde in 0.1M sodium cacodylate buffer, pH7.4, and testes post-fixed

overnight in the same fixative. Samples were then placed in 2% osmium tetroxide in 0.1M PBS pH 7.4, dehydrated in a graded series of ethyl alcohol and embedded in Durcupan resin. Ultrathin sections of 80nm were cut with a Reichert-Jung UltracutE ultramicrotome and placed on formvar-coated slot copper grids. Sections were counterstained with uranyl acetate and lead citrate and viewed with a FEI Tecnai12 BioTwinG^2 electron microscope. Digital images were acquired with an AMT XR-60 CCD Digital Camera system and compiled using Adobe Photoshop.

Supplementary Material

Refer to Web version on PubMed Central for supplementary material.

Acknowledgments

We thank Drs. S. Chuma (Kyoto U.), R. Jessberger (Dresden U. Tech.), A. Vasileva (Mt. Sinai), S. K-Miyagawa and T. Nakano (Osaka U.), and C. Chen and T. Pawson (Samuel Lunenfeld Res. Inst.) for the kind gifts of piRNA pathway expression plasmids, Dr. A. Newton for the DAG sensor, B. Cyge for advice, and many colleagues for critical manuscript feedback. Supported by NIH GM071520 and GM084251 to MAF, GM50388 and P20RR021954 to AJM, and fellowships from NIH (T32-DK07521) and AHA to QG and HR.

References

Aravin AA, van der Heijden GW, Castaneda J, Vagin VV, Hannon GJ, Bortvin A. Cytoplasmic compartmentalization of the fetal piRNA pathway in mice. PLoS Genet. 2009; 5:e1000764. [PubMed: 20011505]

Brennecke J, Aravin AA, Stark A, Dus M, Kellis M, Sachidanandam R, Hannon GJ. Discrete small RNA-generating loci as master regulators of transposon activity in Drosophila. Cell. 2007; 128:1089–1103. [PubMed: 17346786]

Brindley DN, Pilquil C, Sariahmetoglu M, Reue K. Phosphatidate degradation: phosphatidate phosphatases (lipins) and lipid phosphate phosphatases. Biochim Biophys Acta. 2009; 1791:956–961. [PubMed: 19250975]

Cazzolli R, Shemon AN, Fang MQ, Hughes WE. Phospholipid signaling through phospholipase D and phosphatidic acid. IUBMB life. 2006; 58:457–461. [PubMed: 16916782]

Chen H, Chan DC. Mitochondrial dynamics-fusion, fission, movement, and mitophagy-in neurodegenerative diseases. Hum Mol Genet. 2009; 18:R169–176. [PubMed: 19808793]

Chen H, Detmer SA, Ewald AJ, Griffin EE, Fraser SE, Chan DC. Mitofusins Mfn1 and Mfn2 coordinately regulate mitochondrial fusion and are essential for embryonic development. J Cell Biol. 2003; 160:189–200. [PubMed: 12527753]

Choi SY, Huang P, Jenkins GM, Chan DC, Schiller J, Frohman MA. A common lipid links Mfn-mediated mitochondrial fusion and SNARE-regulated exocytosis. Nat Cell Biol. 2006; 8:1255–1262. [PubMed: 17028579]

Colley WC, Sung TC, Roll R, Jenco J, Hammond SM, Altshuller Y, Bar-Sagi D, Morris AJ, Frohman MA. Phospholipase D2, a distinct phospholipase D isoform with novel regulatory properties that provokes cytoskeletal reorganization. Curr Biol. 1997; 7:191–201. [PubMed: 9395408]

Du G, Huang P, Liang BT, Frohman MA. Phospholipase D2 localizes to the plasma membrane and regulates angiotensin II receptor endocytosis. Mol Biol Cell. 2004; 15:1024–1030. [PubMed: 14718562]

Finck BN, Gropler MC, Chen Z, Leone TC, Croce MA, Harris TE, Lawrence JC Jr, Kelly DP. Lipin 1 is an inducible amplifier of the hepatic PGC-1alpha/PPARalpha regulatory pathway. Cell Metab. 2006; 4:199–210. [PubMed: 16950137]

Frank S, Gaume B, Bergmann-Leitner ES, Leitner WW, Robert EG, Catez F, Smith CL, Youle RJ. The role of dynamin-related protein 1, a mediator of mitochondrial fission, in apoptosis. Dev Cell. 2001; 1:515–525. [PubMed: 11703942]

Giorgione JR, Lin JH, McCammon JA, Newton AC. Increased membrane affinity of the C1 domain of protein kinase Cdelta compensates for the lack of involvement of its C2 domain in membrane recruitment. J Biol Chem. 2006; 281:1660–1669. [PubMed: 16293612]

Han GS, Carman GM. Characterization of the human LPIN1-encoded phosphatidate phosphatase isoforms. J Biol Chem. 2010; 285:14628–14638. [PubMed: 20231281]

He Z, Kokkinaki M, Pant D, Gallicano GI, Dym M. Small RNA molecules in the regulation of spermatogenesis. Reprod. 2009; 137:901–911.

Hosokawa M, Shoji M, Kitamura K, Tanaka T, Noce T, Chuma S, Nakatsuji N. Tudor-related proteins TDRD1/MTR-1, TDRD6 and TDRD7/TRAP: domain composition, intracellular localization, and function in male germ cells in mice. Dev Biol. 2007; 301:38–52. [PubMed: 17141210]

Huang H, Frohman MA. Lipid signaling on the mitochondrial surface. Biochim Biophys Acta. 2009; 1791:839–844. [PubMed: 19540356]

Jenkins GM, Frohman MA. Phospholipase D: a lipid centric review. Cell Mol Life Sci. 2005; 62:2305–2316. [PubMed: 16143829]

Langner CA, Birkenmeier EH, Roth KA, Bronson RT, Gordon JI. Characterization of the peripheral neuropathy in neonatal and adult mice that are homozygous for the fatty liver dystrophy (fld) mutation. J Biol Chem. 1991; 266:11955–11964. [PubMed: 2050689]

Lebiedzinska M, Szabadkai G, Jones AW, Duszynski J, Wieckowski MR. Interactions between the endoplasmic reticulum, mitochondria, plasma membrane and other subcellular organelles. Intl J Biochem & Cell Biol. 2009; 41:1805–1816.

Liu X, Weaver D, Shirihai O, Hajnoczky G. Mitochondrial 'kiss-and-run': interplay between mitochondrial motility and fusion-fission dynamics. EMBO J. 2009; 28:3074–3089. [PubMed: 19745815]

Ma L, Buchold GM, Greenbaum MP, Roy A, Burns KH, Zhu H, Han DY, Harris RA, Coarfa C, Gunaratne PH, et al. GASZ is essential for male meiosis and suppression of retrotransposon expression in the male germline. PLoS Genet. 2009; 5:e1000635. [PubMed: 19730684]

Malone CD, Brennecke J, Dus M, Stark A, McCombie WR, Sachidanandam R, Hannon GJ. Specialized piRNA pathways act in germline and somatic tissues of the Drosophila ovary. Cell. 2009; 137:522–535. [PubMed: 19395010]

Mor A, Campi G, Du G, Zheng Y, Foster DA, Dustin ML, Philips MR. The lymphocyte function-associated antigen-1 receptor costimulates plasma membrane Ras via phospholipase D2. Nat Cell Biol. 2007; 9:713–719. [PubMed: 17486117]

Nakanishi H, Morishita M, Schwartz CL, Coluccio A, Engebrecht J, Neiman AM. Phospholipase D and the SNARE Sso1p are necessary for vesicle fusion during sporulation in yeast. J Cell Sci. 2006; 119:1406–1415. [PubMed: 16554438]

Namekawa SH, Park PJ, Zhang LF, Shima JE, McCarrey JR, Griswold MD, Lee JT. Postmeiotic sex chromatin in the male germline of mice. Curr Biol. 2006; 16:660–667. [PubMed: 16581510]

Pane A, Wehr K, Schupbach T. zucchini and squash encode two putative nucleases required for rasiRNA production in the Drosophila germline. Dev Cell. 2007; 12:851–862. [PubMed: 17543859]

Paniagua R, Nistal M, Amat P, Rodriguez MC. Presence of ribonucleoproteins and basic proteins in the nuage and intermitochondrial bars of human spermatogonia. J Anat. 1985; 143:201–206. [PubMed: 3870728]

Riebeling C, Morris AJ, Shields D. Phospholipase D in the Golgi apparatus. Biochim Biophys Acta. 2009; 1791:876–880. [PubMed: 19376267]

Rizzo MA, Shome K, Watkins SC, Romero G. The recruitment of Raf-1 to membranes is mediated by direct interaction with phosphatidic acid and is independent of association with Ras. J Biol Chem. 2000; 275:23911–23918. [PubMed: 10801816]

Russell L, Frank B. Ultrastructural characterization of nuage in spermatocytes of the rat testis. Anat Rec. 1978; 190:79–97. [PubMed: 626418]

Saito K, Inagaki S, Mituyama T, Kawamura Y, Ono Y, Sakota E, Kotani H, Asai K, Siomi H, Siomi MC. A regulatory circuit for piwi by the large Maf gene traffic jam in Drosophila. Nature. 2009; 461:1296–1299. [PubMed: 19812547]

Schug ZT, Gottlieb E. Cardiolipin acts as a mitochondrial signalling platform to launch apoptosis. Biochim Biophys Acta. 2009; 1788:2022–2031. [PubMed: 19450542]

Schultz N, Hamra FK, Garbers DL. A multitude of genes expressed solely in meiotic or postmeiotic spermatogenic cells offers a myriad of contraceptive targets. Proc Natl Acad Sci USA. 2003; 100:12201–12206. [PubMed: 14526100]

Soper SF, van der Heijden GW, Hardiman TC, Goodheart M, Martin SL, de Boer P, Bortvin A. Mouse maelstrom, a component of nuage, is essential for spermatogenesis and transposon repression in meiosis. Dev Cell. 2008; 15:285–297. [PubMed: 18694567]

Thomson T, Lin H. The biogenesis and function of PIWI proteins and piRNAs: progress and prospect. Ann Rev Cell Dev Biol. 2009; 25:355–376. [PubMed: 19575643]

Twig G, Elorza A, Molina AJ, Mohamed H, Wikstrom JD, Walzer G, Stiles L, Haigh SE, Katz S, Las G, et al. Fission and selective fusion govern mitochondrial segregation and elimination by autophagy. EMBO J. 2008; 27:433–446. [PubMed: 18200046]

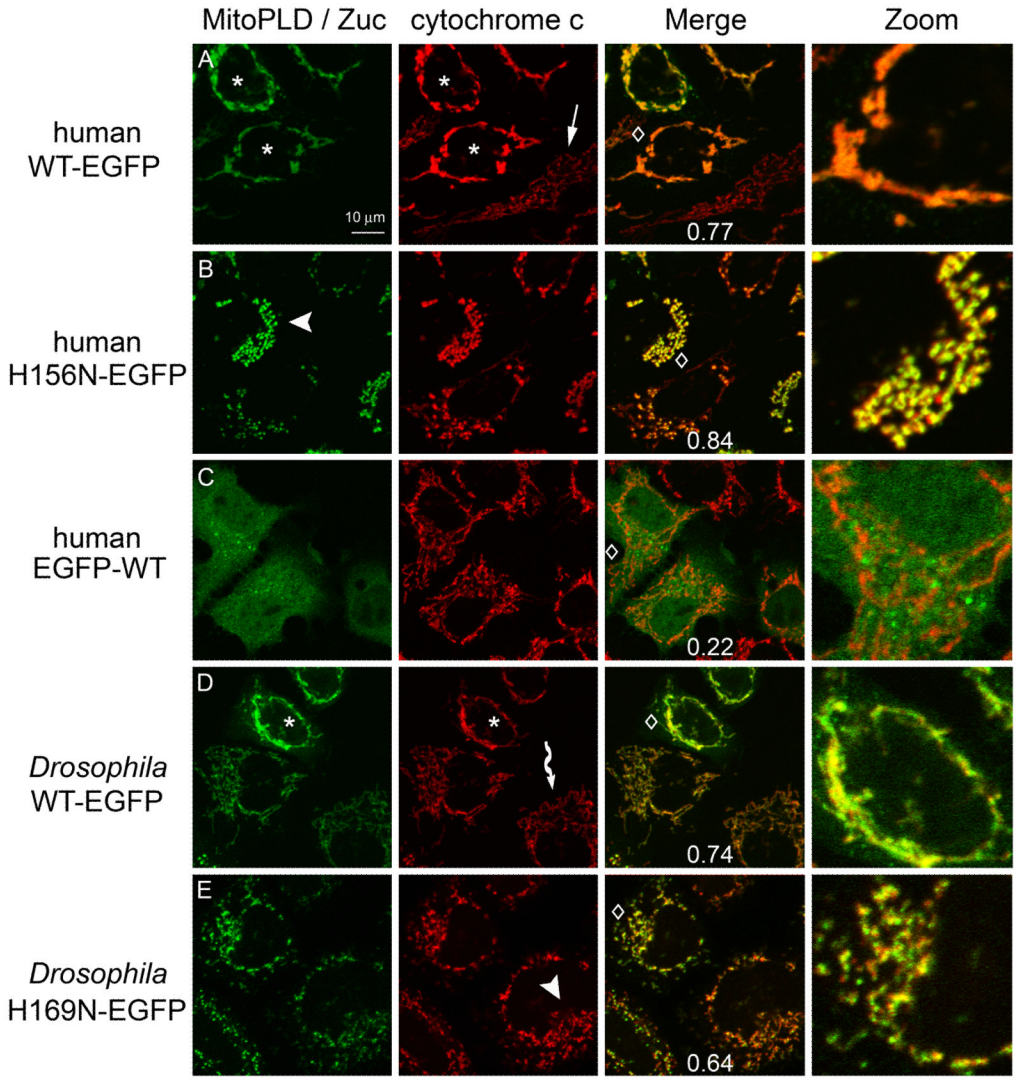

Fig. 1. *Drosophila* Zuc localizes to and aggregates mitochondria in an activity-dependent manner

HeLa cells were transiently transfected with expression plasmids for tagged isoforms of human MitoPLD and *Drosophila* Zuc, immunostained for cytochrome (cyt) c to visualize mitochondria, and imaged using confocal microscopy. (A) WT MitoPLD C-terminally tagged with EGFP; (B) Catalytically-inactive (H156N) MitoPLD; (C) WT MitoPLD N-terminally tagged with EGFP; (D) Zuc C-terminally tagged with EGFP; (E) Catalytically-inactive (H169N) Zuc. *, transfected cells with mitochondrial aggregation; arrow, non-transfected cell with tubular mitochondria; diamond, region magnified zoomed panel; arrowhead, fragmented mitochondria; wavy arrow, co-localization of Zuc with mitochondrial tubules at low levels of expression. The cells shown are typical of those observed in multiple fields for transfection experiments performed 3 or more times. Co-localization coefficients for transfected cells shown are shown at the bottom of the merged panels, using the range 0 (no co-localization) to 1 (all pixels co-localized) to indicate the degree of co-localization of MitoPLD / Zuc with cyt c.

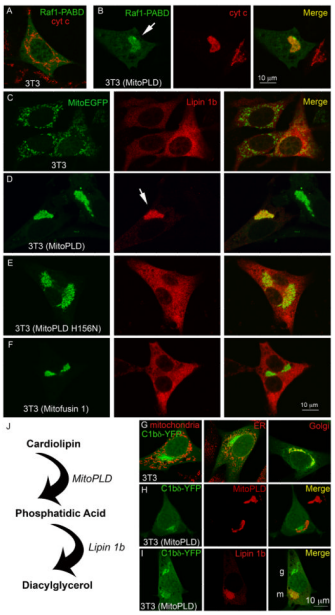

Fig. 2. Lipin 1b is recruited to the mitochondrial surface by MitoPLD-generated PA which it converts to DAG

(A, B) MitoPLD-generated PA can be detected by a cytosolic PA sensor. Control (A) and inducible-MitoPLD-expressing (B) NIH3T3 cells were transfected with an expression plasmid encoding the Raf1 PA sensor (Raf1-PABD). Arrow, localization of sensor to MitoPLD-aggregated mitochondria. (C–F) Activity-dependent recruitment of Lipin 1b to mitochondria by MitoPLD. NIH3T3 control cells (C) or inducible cells expressing (D) WT MitoPLD, (E) catalytically-inactive H156N-MitoPLD, or (F) Mitofusin 1 were transiently co-transfected with MitoEGFP to visualize mitochondria and HA-tagged Lipin 1b. 1 day later, the cells were immunostained with anti-HA to detect Lipin 1b. Arrow, localization of Lipin 1b to MitoPLD-aggregated mitochondria. (G–I) Production of DAG on the mitochondrial surface following Lipin 1b translocation. (G) Control NIH3T3 cells were transfected with an expression plasmid encoding a DAG sensor (C1bδ-YFP) and immunostained to detect cytochrome c, or calreticulin as an endoplasmic reticulum (ER) marker and GM130 as a Golgi marker. (H) C1bδ-YFP (green) was transiently transfected into NIH3T3 cells expressing MitoPLD-Flag, which was detected using an anti-Flag epitope monoclonal antibody. (I) Co-transfection of HA-Lipin 1b and C1bδ-YFP into NIH3T3 cells expressing MitoPLD-Flag. g, Golgi; m, mitochondria. The cells shown are typical of >90% of the cells in multiple fields for transfection experiments performed 3 or more times. (J) Proposed model for the MitoPLD-Lipin mitochondrial surface lipid signaling pathway.

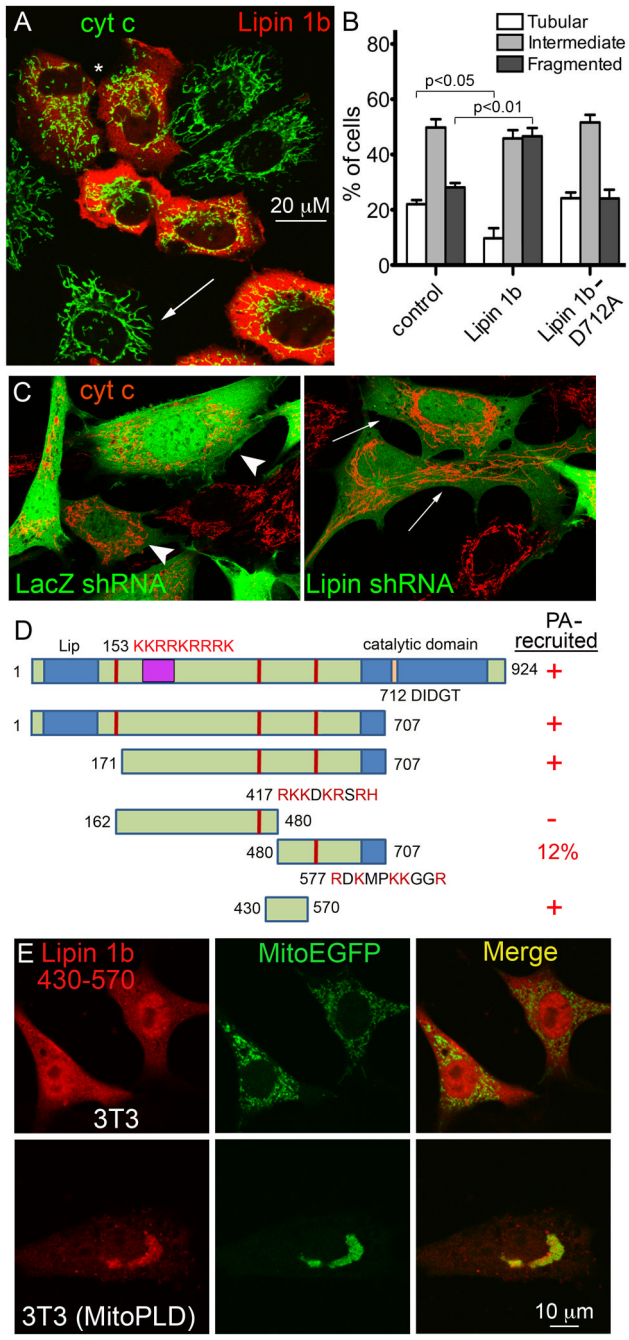

Fig. 3. Lipin 1b is recruited to mitochondria via a central domain and promotes mitochondrial tubule shortening at physiological levels of PA in an activity-dependent manner

(A) Lipin 1b overexpression shortens mitochondrial tubules. HeLa cells were transiently transfected with control vector, wild-type HA-Lipin 1b, or catalytically-inactive HA-Lipin 1b-D712A. 24 hours later, the cells were stained with anti-HA antibody (red) and cyt c (green). Asterisk, transfected cells with fragmented mitochondria; arrow, non-transfected cell with tubular mitochondria. (B) Mitochondrial morphology was quantified for cells with predominantly tubular, intermediate, or fragmented mitochondria (see Methods). The experiment was repeated three times with an average of 61 cells counted of each type per experiment. Bars, SD. (C) Knockdown of Lipin 1 using adenoviral-delivered shRNA causes

lengthening of mitochondrial tubules. Left, control NIH3T3 cells infected with Lac Z shRNA. The shRNA vector additionally expresses EGFP to reveal which cells are transfected and the level of transfection. Note that the length of mitochondria as imaged using anti-cyt. C antisera (red) is similar in transfected (arrowheads) versus non-transfected cells. Right panel, NIH3T3 cells infected with Lipin 1 shRNA. Note the elongated mitochondria (arrows). The experiment was performed three times, counting 100 cells in each condition per experiment. (D–E) PA-dependent translocation depends on a central region of Lipin 1b. Deletion mutants of Lipin 1b were co-transfected with MitoEGFP into control and MitoPLD-expressing NIH3T3 cells and imaged as shown in Fig. 2C and D to identify the region that mediates PA-induced translocation to mitochondria. “+”, translocation seen in >95% of co-transfected cells; “-“, no translocation observed. n>100 cells for each construct, which were transfected in at least three separate experiments. Red lines, basic amino acid clusters; purple box, alternate exon included in Lipin 1b and excluded in Lipin 1a; yellow bar, catalytic motif. (E) Lipin 1b (430–570) and MitoEGFP co-transfected into control and MitoPLD-expressing NIH3T3 cells.

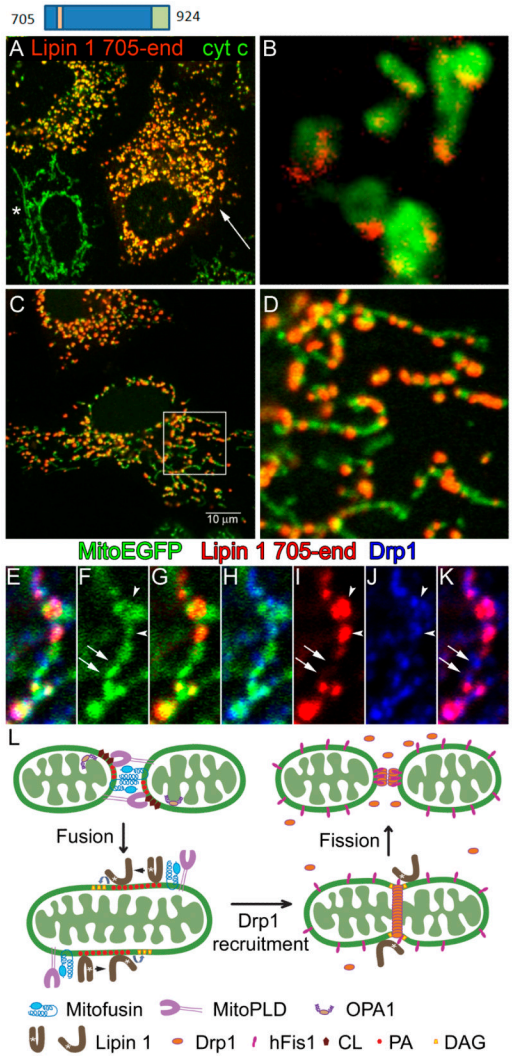

Fig. 4. The Lipin 1 catalytic domain translocates independently of PA to sites of mitochondrial fission and causes mitochondrial fragmentation

(A–D) HeLa cells were transfected with Lipin 1b 705-end. (A) Asterisk, non-transfected cell showing normal mitochondrial tubulation. Arrow, transfected cells with extensive fragmentation. (B) Magnification of fragmented tubules. Note the localization of HA-Lipin 1b to the tips of the fragments. (C) Example of a relatively infrequent (13% ± 1.9%) transfected cell that retained some tubulation. (D) Magnification of tubules decorated with HA-Lipin 1b. (E–K) Co-localization of HA-Lipin 1b with endogenous Drp1 on tubules (lower power magnifications, Fig. S4C). (F, I, K) Arrowheads, constrictions with Drp1 and the Lipin 1 catalytic domain. (F,I,K) Arrows, constrictions with only Drp1. (L) Proposed model for regulated mitochondrial fusion and subsequent fission. Production of PA by MitoPLD facilitates mitochondrial fusion followed by the recruitment of Lipin 1 to convert the PA into DAG, which promotes fission at nearby sites. See text for details.

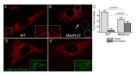

Fig. 5. Loss of MitoPLD shortens mitochondrial tubules in mouse embryo fibroblasts

(A) MEFs prepared from WT and MitoPLD$^{-/-}$ day 13.5 embryos were fixed, immunostained for cyt c, and scored for tubular morphology. (A) Typical fully-tubulated WT MEF. (B) Typical MitoPLD$^{-/-}$ MEF with shortened tubules and many mitochondrial fragments (arrow), particularly in periphery of cell. Thin circle, region containing mitochondrial fragments copied into thick circle with increased brightness. (C) Quantitation of mitochondrial morphologies. MitoPLD$^{-/-}$ MEFs generally displayed at least a small amount of tubulation and thus were scored as intermediate rather than fragmented, despite obvious differences in appearance of the tubules. The experiment was performed 5 times with an average of 61 cells counted of each type per experiment. Bars, SD. (D,E) Transient transfection of Lipin 1b 705-end in WT and MitoPLD$^{-/-}$ MEFs causes extensive fragmentation in both cell lines.

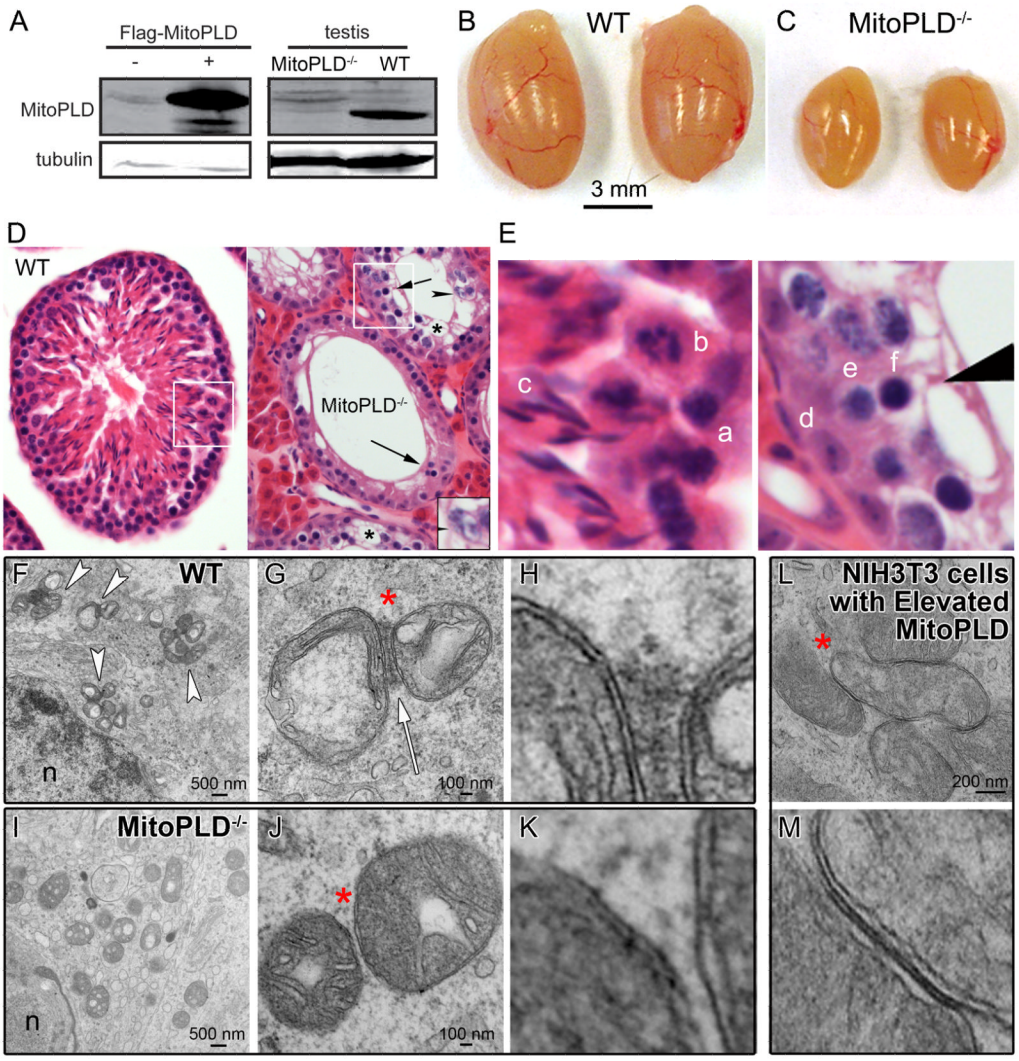

Fig. 6. MitoPLD$^{-/-}$ mice exhibit meiotic arrest during spermatogenesis and loss of nuage

(A) MitoPLD is expressed in testes. An affinity-purified anti-MitoPLD peptide rabbit antiserum that recognizes MitoPLD overexpressed in NIH3T3 cells (left panel) by Western blotting identifies a band of the correct size (35 kDa) in WT testes (right panel) that is absent in MitoPLD$^{-/-}$ testes. Tubulin, loading control. (B,C) MitoPLD$^{-/-}$ testes were uniformly reduced in size compared to WT testes (n>20). (D) Hematoxylin and eosin staining of testes sections. White boxes, areas magnified in (E); asterisks, vacuole / cell drop-out sites; arrow, apoptotic cell with condensed, darkly staining nucleus; arrowhead, cell with disorganized chromosomal material (magnified in inset at lower right of panel). (E) Insets from (D). a and e, prophase spermatocyte; b, meiotic spermatocyte; c, spermatid; d, spermatogonia; f, apoptotic cell (below) and cell with disorganized chromosomal material (above). (F–K) Electron microscopy of WT (F–H) and MitoPLD$^{-/-}$ (I–K) testes. n, nucleus; arrowheads, nuage associated with aggregated mitochondria; arrow, nuage; asterisk, magnified region in (H,K,M). (L,M) NIH3T3 cells expressing elevated levels of MitoPLD. Images presented in (D–K) are representative of > 400 images collected from 2–3 mice per genotype in different experiments. Mice were 2–4 months in age.

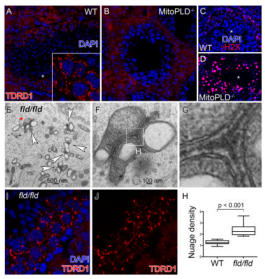

Fig. 7. Loss of TDRD1 expression and increased double-strand breaks in MitoPLD$^{-/-}$ testes, whereas *fld/fld* testes exhibit increased nuage and altered TDRD1 localization

(A,B) Frozen sections of WT and MitoPLD$^{-/-}$ testes were fixed and stained with DAPI and immunostained with anti-TDRD1. Inset, magnification of area indicated by asterisk. Diffuse red haze in interstitial tissue in WT and MitoPLD$^{-/-}$ testes reflects non-specific staining. (C, D) Frozen sections were stained with DAPI and immunostained with anti-γH2X. Images representative of >40 sections examined from two separate immunostaining experiments. All images were captured with the same intensity of laser and processed identically. Asterisk, center of tubule. (E–G) Electron microscopy images of *fld/fld* testes. Arrowheads, nuage; asterisk, white box, areas magnified in (F,G). Representative of >75 images from 3 adult (2–4 month old) mice. (H) Normalized nuage density in WT and *fld/fld* testes. NIH ImageJ software was used to quantitate nuage density, which was then normalized to the density of adjacent mitochondrial matrix to control for contrast and darkness of image (compare panel H to Fig. 6H). n=21 measurements for each genotype, images obtained from multiple grids and experiments. Box, 25th and 75th percentiles; bars, range. (I,J) Anti-TDRD1 and DAPI staining in frozen sections from *fld/fld* testes. n=2 experiments, 5 sections / experiment. Representative images.